# Copolar Calibration of Multistatic Radar in the Presence of Multipath

Riccardo Palamà, Maria Greco, Fulvio Gini
Dipartimento di Ingegneria dell'Informazione
Università di Pisa, Pisa, Italy
riccardo.palama@gmail.com,
{maria.greco;f.gini@iet.unipi.it}

Francesco Fioranelli, Matthew Ritchie, Hugh Griffiths
Department of Electronic and Electrical Engineering
University College London
London, UK

***Abstract* — This paper addresses the polarimetric calibration of the nodes of a multistatic radar system, by using a reference object with known scattering matrix, such as a metallic sphere. A calibration technique is proposed and its experimental validation performed in a realistic scenario, by accounting also for the multipath effect. The intensity of the signal scattered by a metallic sphere and received by the monostatic and bistatic nodes of the NetRAD system is measured, by varying the antenna height, the object range and the bistatic angle. The adopted calibration technique shows a quite good accuracy, as the calibrated values of the radar cross section of the reference object are close to the theoretical ones, after the compensation of the multipath effect.**

***Keywords—polarimetric calibration; multistatic radar; radar multipath.***

## I. INTRODUCTION

In recent years, there has been an increasing interest on bistatic and multistatic radar systems, consisting of different separate nodes. These systems are able to increase the diversity of a radar system, as they consist of multiple nodes that look at the radar scene from different aspect angles. In addition to this 'geometric diversity', a further degree of freedom can be achieved by combining the radar returns at different transmitter-receiver polarizations. However, the fusion of polarimetric returns should be preceded by a calibration stage, which aims at correcting errors and non-idealities introduced by the antennas. This problem is commonly known as *polarimetric calibration*, and has been deeply studied for monostatic radar systems [1-3].

A possible method consists of using one or more objects with known scattering matrix as reference. One of the most common reference objects for monostatic calibration is the trihedral corner reflector, due to its high radar cross section (RCS). Unfortunately, the trihedral corner reflector cannot be used for bistatic calibration, since its RCS decreases rapidly with increasing bistatic angles [4-7]. A suitable object for bistatic and multistatic calibration is the metallic sphere, as its RCS is not geometry-dependent [8].

To the best of our knowledge, there is little available work addressing the polarimetric calibration of bistatic/multistatic radar nodes, and they tend to deal with *quasi*-monostatic cases, i.e. bistatic geometries with small bistatic angles. In this work, we aim at proposing a polarimetric calibration technique for a multistatic radar system deployed to achieve significant bistatic angles. An experimental validation of the proposed technique is performed by using the UCL NetRAD system, in a realistic scenario. NetRAD is a multistatic coherent pulse radar with three separate but identical nodes operating at 2.4 GHz, S-band. This system has been developed in the past few years at University College London [9] and has been employed for different research applications, such as sea clutter analysis [10], micro-UAV detection and classification [11], and human micro-Doppler characterization [12].

The measurements highlight the presence of a strong multipath effect, due to multiple reflections of the scattered signal on the ground plane. A model to compensate for the multipath effect is adopted in this paper, taking into account the system geometry and the electromagnetic (e.m.) scattering properties of the reflecting plane [13-14]. The multistatic calibration technique and the proposed multipath model are evaluated using co-polarized data in this paper.

This paper is organized as follows: Section II illustrates the theoretical foundations of the proposed multistatic polarimetric calibration method. Section III describes the radar system and the realized experiments. Section IV discusses the results obtained before and after the multipath compensation. Final remarks are drawn in Section V.

## II. MULTISTATIC POLARIMETRIC CALIBRATION

### A. Received Signal Model

The electric field received by radar antenna in the presence of a target consists of four complex components, two co-polar ($E_{vv}$ and $E_{hh}$) and two cross-polar ($E_{vh}$ and $E_{hv}$). In the adopted notation, the first and second indexes denote the polarization of the transmitted and received signal, respectively. The amplitude of each component is indicated as $A_{pq}$ ($p,q = h,v$). The indexes $p$ and $q$ represent the wave polarization and are set as '$h$', indicating the horizontal polarization, or '$v$', indicating the vertical polarization. The resulting model is given by

$$\mathbf{E} = \begin{bmatrix} E_{vv} & E_{vh} \\ E_{hv} & E_{hh} \end{bmatrix} = e^{-j2kD} \frac{1}{D^2} K\mathbf{RST} \qquad (1)$$

where $K$ is a constant term, accounting for the system parameters, i.e $K=\sqrt{P_T G_T G_R \lambda (4\pi)^{-3}}$ . $G_T$ and $G_R$ are the gain of the transmitter and receiver antenna, respectively. $P_T$ is the transmitted power, $D$ is the monostatic range, $k$ is the wavenumber, and $\mathbf{S}$ is the target scattering matrix. The scattering matrix of an object is commonly defined as a 2x2 complex matrix, where the generic element $S_{pq} = s_{pq} \exp(j\varphi_{pq})$ is the scattering complex amplitude of the object illuminated by a *p*-polarized e.m. wave and re-irradiating a *q*-polarized e.m. wave.

$$\mathbf{S} = \begin{bmatrix} S_{vv} & S_{vh} \\ S_{hv} & S_{hh} \end{bmatrix} = e^{j\varphi_{vv}} \begin{bmatrix} s_{vv} & s_{vh} e^{j\varphi'_{vh}} \\ s_{hv} e^{j\varphi'_{hv}} & s_{hh} e^{j\varphi'_{hh}} \end{bmatrix} \quad (2)$$

where $\varphi'_{pq} = \varphi_{pq} - \varphi_{vv}$

It should be noted that the radar cross section of an object that receives a *p*-polarized wave and re-irradiates a *q*-polarized wave is related to the scattering amplitude $S_{pq}$ by

$$RCS_{pq} = 4\pi \left| S_{pq} \right|^2 = 4\pi s_{pq}^2 \quad (3)$$

The matrix $\mathbf{T}$ represents the transmitter distortion matrix,

$$\mathbf{T} = \begin{bmatrix} T_{vv} & T_{vh} \\ T_{hv} & T_{hh} \end{bmatrix} \quad (4)$$

where the terms $T_{vv}$ and $T_{hv}$ indicate the system distortions for the vertically-polarized transmit mode. Under ideal conditions, if the *h* and *v* ports of the transmitter antenna are not coupled, then $T_{vv}$ = 1 and $T_{hv}$ = 0. Under non-ideal conditions we have $T_{vv}$<1, due to amplitude and phase errors in the transmitted signal, and $T_{hv}$>0, due to the coupling between the *h* and *v* ports of the antenna. In the case of horizontally-polarized transmit mode, $T_{hh}$ and $T_{vh}$ represent the copolar and cross-polar distortion, respectively. The receiver distortion matrix is

$$\mathbf{R} = \begin{bmatrix} R_{vv} & R_{vh} \\ R_{hv} & R_{hh} \end{bmatrix} \quad (5)$$

where $R_{vv}$ and $R_{hh}$ represent amplitude and phase distortions introduced by the receiver antenna ($R_{vv}$, $R_{hh}$ equal to 1, in the ideal case) and $R_{hv}$, $R_{vh}$ represent cross-polarization coupling (both equal to zero in the ideal case).

In this work, we deal with a simple distortion model, assuming that there is no coupling between the *h* and *v* ports of both the transmitter and receiver. In this case, both the matrices $\mathbf{R}$ and $\mathbf{T}$ are diagonal, i.e. $R_{hv} = R_{vh} = T_{hv} = T_{vh} = 0$. Furthermore, we only consider the amplitude of the received signal as phase calibration is beyond the scope of this paper. The received signal model resulting from the aforementioned assumptions about the system distortions is given by

$$\mathbf{E} = e^{-j2kD} \frac{1}{D^2} K \begin{bmatrix} T_{vv} S_{vv} R_{vv} & T_{vv} S_{vh} R_{hh} \\ T_{hh} S_{hv} R_{vv} & T_{hh} S_{hh} R_{hh} \end{bmatrix} \quad (6)$$

In this case, the calibration problem is usually referred to as *simple polarimetric calibration*, which has been solved for monostatic radars by using two reference objects. A reasonable choice of these two calibration objects includes a first object with a known diagonal scattering matrix and a second object with an unknown full scattering matrix [1-2]. If the aforementioned assumptions do not apply, the problem can be solved by using three objects, and possible solutions are illustrated in [3].

### *B. Polarimetric Multistatic Calibration*

In this work, we use a multistatic system that consists of a monostatic node - with parameters denoted by the index *m* - and a bistatic node - with parameters denoted by the index *b*. The transmitter distortion matrix is the same for all receiver-transmitter pairs, as there is only one transmitter. On the other hand, the receiver distortion matrices of the system nodes cannot be assumed to be identical. Hence, in the following received signal model, the matrix $\mathbf{T}_m$ is used for both the monostatic and bistatic nodes, whereas $\mathbf{R}_m$ and $\mathbf{R}_b$ denote the receiver distortion matrices of the monostatic node and of the bistatic node, respectively. The received electric fields of the monostatic and bistatic nodes are given by

$$\mathbf{E}_m = e^{-j2kD_m} \frac{1}{D_m^2} K_m \mathbf{R}_m \mathbf{S}_m \mathbf{T}_m \quad (7)$$

$$\mathbf{E}_b = e^{-jk(D_m + D_b)} \frac{1}{D_m D_b} K_b \mathbf{R}_b \mathbf{S}_b \mathbf{T}_m \quad (8)$$

The constant terms $K_m$ and $K_b$ are given by

$$K_m = \left( P_T G_T G_R^{(m)} \lambda (4\pi)^{-3} \right)^{1/2} \text{ and } K_b = \left( P_T G_T G_R^{(b)} \lambda (4\pi)^{-3} \right)^{1/2}$$

Note that $P_T$, $G_T$ and $\lambda$ are fixed parameters, as they are only related to the transmitter. The parameters $G_R^{(m)}$ and $G_R^{(b)}$ represent the gain of the receiver antennas of the monostatic and bistatic nodes, respectively. As shown in Fig.1, the target is located at a distance $D_m$ from the monostatic node and at a distance $D_b$ from the bistatic node. The resulting bistatic angle is $\beta$. It should be noted that, if the calibration object is *accurately aligned*, the monostatic range and the bistatic range are known.

After performing the polarimetric calibration of the monostatic node with one of the methods illustrated in [1-3] and two or three calibration objects, the values of $R_{hh}^{(m)} T_{hh}^{(m)}, R_{hh}^{(m)} T_{vv}^{(m)}, R_{vv}^{(m)} T_{hh}^{(m)}, R_{vv}^{(m)} T_{vv}^{(m)}$ are exactly known, thus the value of the ratio $T_{vv}^{(m)} / T_{hh}^{(m)}$ is also known, and

$$T_{vv}^{(m)} = \alpha T_{hh}^{(m)} \quad (9)$$

By using a reference object with known diagonal bistatic scattering matrix $\mathbf{S}_b \big|_{ref}$ , it is possible to calibrate the bistatic receiver. By using this object as reference for the calibration of the bistatic receiver we can obtain equation (10) and equation (11) by applying equation (9):

$$\begin{cases} T_{vv}^{(m)} R_{vv}^{(b)} = e^{jk(D_m+D_b)} D_m D_b E_{vv}^{(b)} \left( S_{vv} \Big|_{ref} \right)^{-1} = \gamma \\ T_{hh}^{(m)} R_{hh}^{(b)} = e^{jk(D_m+D_b)} D_m D_b E_{hh}^{(b)} \left( S_{hh} \Big|_{ref} \right)^{-1} = \delta \end{cases} \quad (10)$$

$$\begin{cases} T_{vv}^{(m)} R_{hh}^{(b)} = \alpha T_{hh}^{(m)} R_{hh}^{(b)} = \alpha\gamma \\ T_{hh}^{(m)} R_{vv}^{(b)} = \alpha^{-1} T_{vv}^{(m)} R_{vv}^{(b)} = \alpha^{-1}\delta \end{cases} \quad (11)$$

The calibration of the bistatic receiver is complete, as α, γ and δ are known parameters. The sphere is a good candidate for this simple polarimetric calibration, as its scattering matrix is diagonal and does not vary with the geometry.
It should be noted that only the amplitudes of the distortion terms are required to perform an amplitude calibration. They can be computed by extracting the amplitude of each complex term in equation (10) and (11).

*C. Copolar Calibration with Multipath Compensation*

We consider the presence of the multipath component, due to multiple reflections on the ground surface. The model for the amplitude of the received signals, considering only the co-polar components and the multipath effect [13-14] is

$$\begin{cases} A_{pp}^{(m)} = D_m^{-2} K_m \left| R_{pp}^{(m)} T_{pp}^{(m)} \right| s_{pp}^{(m)} M_{pp}^{(m)} \\ A_{pp}^{(b)} = \left( D_b D_m \right)^{-1} K_b \left| R_{pp}^{(b)} T_{pp}^{(m)} \right| s_{pp}^{(b)} M_{pp}^{(b)} \end{cases} \text{ with } p = h,v. \quad (12)$$

It should be noted that in (12) the amplitude of the co-polar distortion components, $R_{pp}^{(m)} T_{pp}^{(m)}$ and $R_{pp}^{(b)} T_{pp}^{(m)}$, is extracted and that the amplitude of the scattering elements - $s_{pp}^{(m)}$ and $s_{pp}^{(b)}$ - is used. The multipath effect, due to multiple reflections from the ground surface, is introduced in the received signal model through the multipath term $M_{pp}$, given by

$$M_{pp}^{(m)} = \left| 1 + \rho_p^{(m)} \exp\left(-j\phi\right) \right|^2 \quad (13)$$

where $p = h,v$ and $\phi$ is the phase deviation between the direct ray and the two-way reflected ray. For the monostatic node, the phase deviation is given by

$$\phi_m = 4\pi h_R h_{TGT} \left( \lambda D_m \right)^{-1} \quad (14)$$

where $h_R$ is the radar antenna height, $h_{TGT}$ is the target height, $\lambda$ is the wavelength. The term $\rho_p$ represents the Fresnel reflection coefficient for a *p*-polarized e.m. wave, summarizing the reflecting properties of the ground surface. The Fresnel reflection coefficient for horizontal polarization, $\rho_h$, is given by

$$\rho_h = \frac{\sin\theta - \sqrt{Y \sin\theta - \cos^2\theta}}{\sin\theta - \sqrt{Y \sin\theta - \cos^2\theta}} \quad (15)$$

In the case of vertical polarization, $\rho_v$ is given by

$$\rho_v = \frac{Y^2 \sin\theta - \sqrt{Y^2 \sin\theta - \cos^2\theta}}{Y^2 \sin\theta - \sqrt{Y^2 \sin\theta - \cos^2\theta}} \quad (16)$$

where $\theta$ is the grazing angle of the reflection point located on the ground plane [1]. A sketch of the system geometry on the elevation plane is shown in Fig.2. The monostatic grazing angle is given by

$$\theta_m = \arctan\left[ \left( h_R + h_{TGT} \right) / D_m \right] \quad (17)$$

The parameter *Y* accounts for the electromagnetic properties of the reflecting plane is given by

$$Y = \sqrt{\varepsilon_r - j60\lambda\sigma} \quad (18)$$

where $\varepsilon_r$ is the relative permittivity and $\sigma$ is the conductivity. The value of $\varepsilon_r$ depends on the material of the reflecting plane, in our case soil covered by grass. The soil moisture has also an effect on the value of $\varepsilon_r$, as the presence of water increases the electrical permittivity of materials [1]. Depending on the soil moisture, values of $\varepsilon_r$ are included between 0 and 40. The conductivity has low values, approximately equal to 0.01 S/m.
For the bistatic geometry, the e.m. wave is reflected around two different points on the ground plane. The first reflecting point is the same as in the monostatic geometry, characterized by the Fresnel coefficient $\rho_p^{(m)}$ and phase deviation $\phi_m$ .The second reflecting point is located along the path from the target to the bistatic node, characterized by a phase deviation given by

$$\phi_b = 4\pi h_R h_{TGT} \left( \lambda D_b \right)^{-1} \quad (19)$$

whereas the Fresnel reflection coefficient, $\rho_p^{(b)}$, is obtained from (15) or (16), by using the grazing angle $\theta_b = \arctan\left[ \left( h_R + h_{TGT} \right) / D_b \right]$ of the reflection point between the target and the bistatic node.
The resulting bistatic multipath coefficient is given by

$$M_{pp}^{(b)} = \left| 1 + \rho_p^{(m)} \mathrm{e}^{-j\varphi_m} + \rho_p^{(b)} \mathrm{e}^{-j\phi_b} + \rho_p^{(m)} \rho_p^{(b)} \mathrm{e}^{-j(\phi_m+\phi_b)} \right| \quad (20)$$

The bistatic antenna height is assumed to be equal to the monostatic one, and $D_b$ represents the bistatic range, i.e. $D_b = \sqrt{D_m^2 + L^2}$ , *L* is the baseline.
The amplitudes of the co-polar elements of the object scattering matrix are calculated by using a reference object of known scattering elements ( $s_{pp}^{(m)}\Big|_{ref}$ , $s_{pp}^{(b)}\Big|_{ref}$ ),

$$\begin{cases} s_{pp}^{(m)} = \dfrac{A_{pp}^{(m)}}{A_{pp}^{(m)}\Big|_{ref}} \left( \dfrac{D_m}{D_m\Big|_{ref}} \right)^2 \dfrac{M_{pp}^{(m)}\Big|_{ref}}{M_{pp}^{(m)}} s_{pp}^{(m)}\Big|_{ref} \\ s_{pp}^{(b)} = \dfrac{A_{pp}^{(b)}}{A_{pp}^{(b)}\Big|_{ref}} \left( \dfrac{D_m D_b}{D_m\Big|_{ref} D_b\Big|_{ref}} \right)^2 \dfrac{M_{pp}^{(b)}\Big|_{ref}}{M_{pp}^{(b)}} s_{pp}^{(b)}\Big|_{ref} \end{cases} \quad (21)$$

In (21) the amplitude of the received electric field from the object under test is normalized to the amplitude of the received electric field of the reference object. The reference object and object under tests can be located at different

distances from the radar nodes, hence their scattered signals are attenuated by different propagation losses and distorted by different multipath terms. These are corrected by the second and third terms in equation (21).

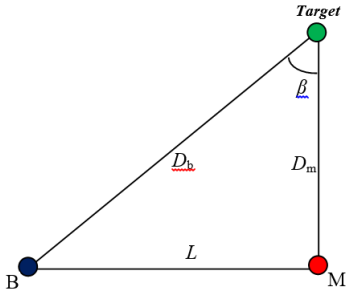


Fig. 1. Sketch of the geometry on the azimuth plane: *M* and *B* are the monostatic and bistatic node, respectively. *L* is the baseline, $D_m$ is the target monostatic range, $D_b$ is the distance of the target from the bistatic node. $\beta$ is the bistatic angle.

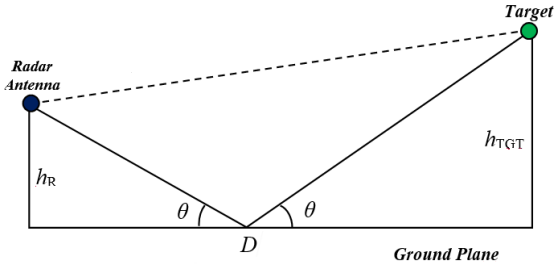


Fig. 2. Sketch of the geometry on the elevation plane: $h_R$ and $h_{TGT}$ are the height of the radar antenna and of the target, respectively. *D* is the distance between the target and the radar antenna, measured on the ground plane. $\theta$ is the grazing angle of the reflection point.

## III. Experiment Description

The experiments used two NetRAD nodes, a monostatic transceiver and a receive-only bistatic receiver. The radar carrier frequency is 2.4 GHz, the pulse repetition frequency (PRF) was set at 1 KHz, and the transmitted signal was a linear up-chirp with 45 MHz bandwidth and 0.6 μs pulse length. Each dataset was 5 s long, with 5000 recorded pulses. The experiment took place in an open football field at the UCL Sports Grounds in Shenley, to the North of London. Fig. 3 shows the calibration targets. A metallic sphere with 40 cm radius was used as a reference object for the bistatic and monostatic measurements. The scattering matrix of a metallic sphere is diagonal, i.e. its cross-polar components are null, whereas its co-polar components (HH and VV) are equal and constant for all the possible geometries. The theoretical RCS of a sphere is given by the area of its section, i.e.

$$RCS_{sphere} = \pi r^2 \qquad (22)$$

The theoretical RCS of the sphere used here was therefore approximately -2.98 dBsm. However, the bistatic sphere RCS can present fluctuations up to several dBs, depending on the ratio of its radius over the wavelength. Furthermore, large values of the bistatic angle require sufficiently large value of radius/wavelength ratio to ensure that the sphere RCS fluctuations are negligible. For this reason a tradeoff between the minimum sphere radius and the maximum bistatic angle should be achieved. After an examination of the RCS fluctuations as a function of the bistatic angle and of the values of this ratio [8], and considering that the sphere radius is equal to 40 cm and the radar wavelength is equal to 12.5 cm, the maximum bistatic angle is approximately 60°.

A trihedral corner reflector was used as a target for the monostatic measurements. The scattering matrix of the trihedral is diagonal and its co-polar components are equal in the monostatic case. Furthermore, its theoretical RCS is very high, thus it is a suitable reference object for calibrating a monostatic radar. The utilized trihedral has square plates, with the side of length *l*, equal to 50 cm. The theoretical RCS of a trihedral with square plates is given by equation (23), approximately equal to 21.7 dBsm for the trihedral used here.

$$RCS_{\text{trihedral}} = 12\pi \frac{l^4}{\lambda^2} \qquad (23)$$

Measurements with different antenna heights and target ranges were performed to evaluate the robustness of the calibration technique against multipath. The baseline was equal to 50 m. A summary of the measurement geometries is illustrated in Table I.

TABLE I. Summary of Measurement Geometries. $H_R$: antenna height, $D_M$: monostatic range, $D_B$: bistatic range, *B*: bistatic angle, $\Theta_M$: monostatic grazing angle, $\Theta_B$: bistatic grazing angle.

| $h_R$ (m) | $D_m$ (m) | $D_b$ (m) | $\beta$ | $\theta_m$ | $\theta_b$ |
|---|---|---|---|---|---|
| 1.06 | 90 | 103 | 29.1° | 1.31° | 1.14° |
| 1.06 | 100 | 112 | 26.8° | 1.18° | 1.05° |
| 1.06 | 110 | 121 | 24.6° | 1.07° | 0.97° |
| 1.60 | 90 | 103 | 29.1° | 1.65° | 1.44° |
| 1.60 | 100 | 112 | 26.8° | 1.49° | 1.33° |

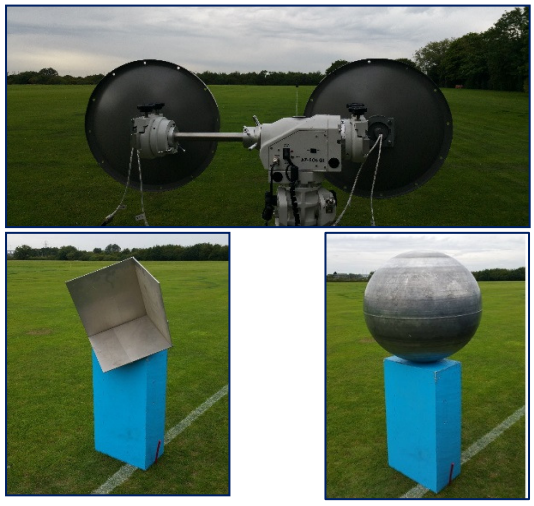

Fig. 3. Antennas at the NetRAD monostatic node and calibration objects (trihedral corner reflector and metallic sphere) mounted on a support of e.m. absorbing material.

After collecting the scattered electric field by the sphere and the trihedral, one of the dataset was chosen as reference and the calibration was performed on the remaining dataset. The difference between the theoretical and the calibrated RCS value was selected as a measure of the calibration accuracy achieved by the adopted technique.

## IV. Results

The time history plots of the received signal intensity as a function of time are shown in Fig.4. The HH and VV data collected by using the sphere as target show an almost constant intensity, approximately equal to -20 dB, whereas the intensity of the cross polarized (HV) data fluctuates between -35 dB and -40 dB. The background intensity fluctuates between -35 dB and -50 dB. These results are related to the fact that the scattering matrix of a sphere is diagonal, with identical diagonal elements. Hence, the HH and VV components should assume identical values and the HV and VH components should consist only of background noise. Both of these hypotheses are verified by the data in Fig.4. The difference between the co-polar and cross-polar signal intensities indicates also the polarization isolation of the system, approximately equal to 15 dB. In the following subsections, the accuracy of the proposed calibration technique is evaluated before and after the compensation of the multipath effect.

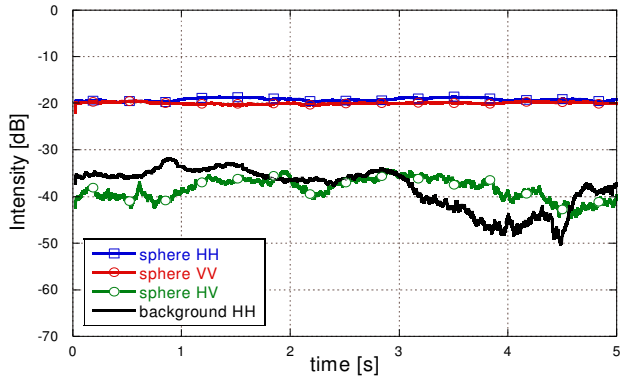


Fig. 4. Time history of intensity values of the received signals (in dB), relative to the bistatic sphere measurements. $h_R$ = 1.06 m and $D_m$ = 90 m.

### A. Before multipath compensation

For each dataset, the mean intensity of the measured data was extracted as an estimate of the signal intensity. The received signal samples as extracted from the range cell where the object was located consist of a constant term, i.e the scattering amplitude of the stationary object, plus a random disturbance. The latter is related to thermal noise and ground clutter, and can be assumed to be Gaussian-distributed. Hence the Maximum-Likelihood Estimate (MLE) of the signal amplitude, $\hat{s}$ is given by equation (24)

$$\hat{s} = \left[ \left( \frac{1}{N} \sum_{n=1}^{N} z_I(n) \right)^2 + \left( \frac{1}{N} \sum_{n=1}^{N} z_Q(n) \right)^2 \right]^{1/2} \qquad (24)$$

where $z_I(n)$ and $z_Q(n)$ represent the in-phase and quadrature received signal samples, respectively. The number of pulses is indicated as N, equal to 5000 for the analyzed datasets.

The measured values of the RCS are calculated as in (3), then calibrated by using (21). The sphere monostatic and bistatic measurements performed at the minimum antenna height (1.06 m) and minimum range from the monostatic node (90 m) were used as reference.

Initially the co-polar calibration was performed without compensating for multipath. The resulting calibrated values of the sphere RCS, compared to the theoretical sphere RCS, are shown in Fig.5.

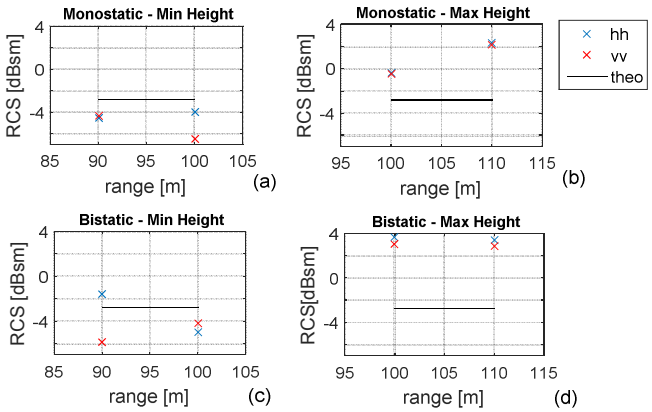


Fig. 5. Calibrated sphere RCS values, before multipath compensation. The HH RCS values are plotted in blue, the VV ones are plotted in red, the theoretical ones in black.

### B. After multipath compensation

A critical parameter for a good multipath model is the relative permittivity, and the variation of the calibrated RCS values as a function of this parameter is shown in Fig. 6. The sphere RCS values are expected to be identical for all the geometries and polarizations. Fig.6a shows that the HH and VV curves cross for $\varepsilon_R \approx 25$ and RCS ≈ -2.55 dBsm. Fig.6b shows that the HH and VV curves cross for $\varepsilon_R \approx 26$ and RCS ≈ -2.4 dBsm. Hence, a good approximation of the permittivity is between 25 and 26. This is confirmed by examining the values of the calibrated RCS values of the trihedral, in the monostatic case as in Fig. 6c, where the HH and VV curves cross for $\varepsilon_R \approx 24$ and RCS ≈ 20.2 dB. The calibrated RCS values, obtained by setting $\varepsilon_R = 25$ are not far from the theoretical values (about -3dBsm for the sphere and 21.7 dBsm for the trihedral).

The calibrated values of the sphere RCS after multipath compensation are shown for each analyzed geometry in Fig.7. By comparing the results shown in Fig.5 and Fig.7, it can be noted that the multipath compensation makes the RCS values closer to the theoretical ones. Except for the monostatic data collected at minimum antenna height and 110 m range, the HH and VV data are almost identical, which shows a good performance of the calibration method in correcting the deviations between data at different polarizations. The calibrated RCS values show deviations smaller than 2.5 dBsm from the theoretical values, meaning

that a good calibration accuracy is achieved, considering that the measurements were realized in a realistic scenario.

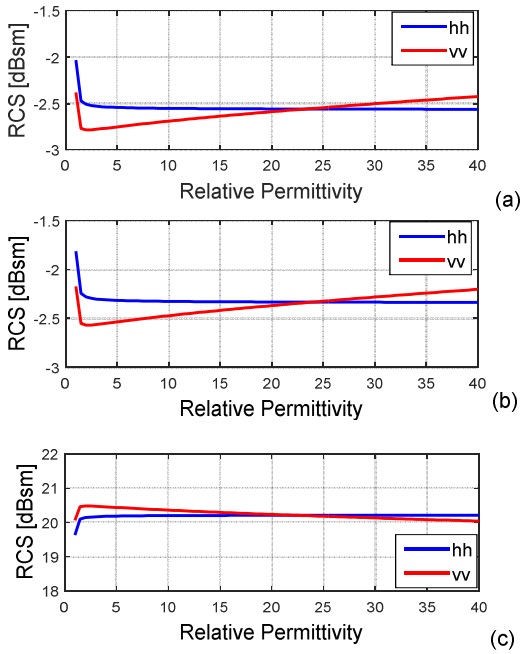


Fig. 6. Calibrated RCS values, after multipath compensation, as a function of the relative permittivity $\varepsilon_R$. Sphere, monostatic (a) and bistatic (b); trihedral monostatic (c), at 100 m monostatic range and maximum antenna height. HH RCS values plotted in blue and VV RCS values plotted in red.

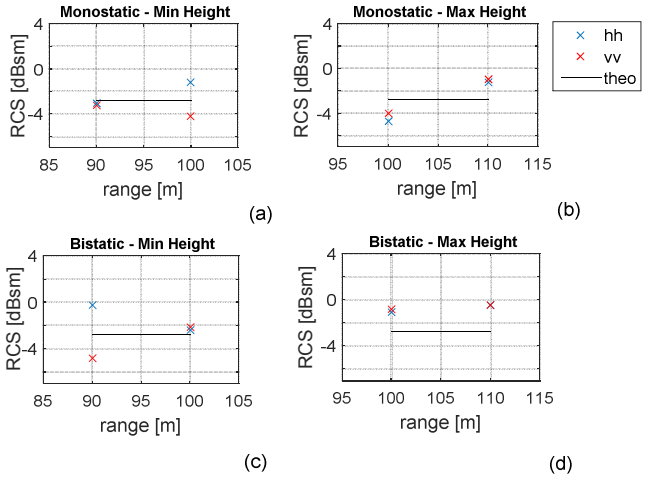


Fig. 7. Calibrated sphere RCS values, after multipath compensation. The HH RCS values are plotted in blue, the VV ones are plotted in red, the theoretical ones in black.

## V. Conclusion

In this work, we have illustrated and tested with experimental data a polarimetric calibration technique for multistatic radar systems. The results obtained from the experimental validation have shown that the calibrated RCS values are almost identical for HH and VV data and that the calibration accuracy is good.

In the future, the proposed calibration technique will be extended to the cross-polar channels, i.e. HV and VH. Furthermore, the assumption on the coupling between the h and v ports of both the receiver and transmitter antennas will be eliminated, in order to realize a fully polarimetric calibration of a multistatic radar. To this aim, one or more objects with totally or partially known bistatic scattering matrix should be found or developed to be used as reference targets for the cross-polar channels.

## Acknowledgment

The authors would like to thank Dr. Keith Ward and Prof. Simon Watts for the helpful discussions about the realized experiments. This work was partially funded by the IET A. F. Harvey Prize 2013 awarded to Prof Hugh Griffiths.

## References

[1] Ulaby F.T., Long D.G., *Microwave Radar and Radiometric Remote Sensing*, The University of Michigan Press, 2014.

[2] Sarabandi, K.; Ulaby, F.T.; Tassoudji, M.A., 'Calibration of polarimetric radar systems with good polarization isolation', *IEEE Transactions on Geoscience and Remote Sensing*, vol.28, no.1, pp.70,75, Jan 1990.

[3] Whitt, M.W.; Ulaby, F.T.; Polatin, P.; Liepa, V.V., 'A general polarimetric radar calibration technique', *IEEE Transactions on Antennas and Propagation*, vol.39, no.1, pp.62,67, Jan 1991.

[4] McLaughlin, D.J.; Ren, Z.; Wu, Y., 'A bistatic polarimeter calibration technique', *IEEE Transactions on Geoscience and Remote Sensing*, vol.33, no.3, pp.796-799, May 1995.

[5] Hauck, B.; Ulaby, F.; DeRoo, R., 'Polarimetric bistatic-measurement facility for point and distributed targets', *IEEE Antennas and Propagation Magazine*, vol.40, no.1, pp.31-41, Feb 1998.

[6] Bradley, C.J.; Collins, P.J.; Fortuny-Guasch, J.; Hastriter, M.L.; Nesti, G.; Terzuoli, A.J.; Wilson, K.S., 'An investigation of bistatic calibration techniques', *IEEE Transactions on Geoscience and Remote Sensing*, vol.43, no.10, pp.2185,2191, Oct. 2005.

[7] Bradley, C.J.; Collins, P.J.; Fortuny-Guasch, J.; Hastriter, M.L.; Nesti, G.; Terzuoli, A.J.; Wilson, K.S., 'An investigation of bistatic calibration objects', *IEEE Transactions on Geoscience and Remote Sensing*, vol.43, no.10, pp.2177,2184, Oct. 2005.

[8] DiBeneditto, J.P, *Bistatic Scattering form Conducting Calibration Spheres*, Technical Report AirForce, 1984.

[9] T. E. Derham, S. Doughty, K. Woodbridge, and C. J. Baker, 'Design and evaluation of a low-cost multistatic netted radar system', *IET Radar, Sonar & Navigation*, vol. 1, pp. 362-368, 2007.

[10] R. Palama, M. S. Greco, P. Stinco and F. Gini, "Statistical analysis of bistatic and monostatic sea clutter," in *IEEE Transactions on Aerospace and Electronic Systems*, vol. 51, no. 4, pp. 3036-3054, Oct. 2015.

[11] F. Fioranelli, M. Ritchie, H. Griffiths, H. Borrion, 'Classification of loaded/unloaded micro-drones using multistatic radar', *Electronic Letters*, vol. 51 (22), 22 October 2015.

[12] Fioranelli, F., Ritchie, M., Griffiths, H.; 'Classification of Unarmed/Armed Personnel Using the NetRAD Multistatic Radar for Micro-Doppler and Singular Value Decomposition Features', *IEEE Geoscience and Remote Sensing Letters*, vol.12, no.9, pp.1933-1937, Sep 2015.

[13] Barton, D.K., 'Low-angle radar tracking', *Proceedings of the IEEE* , vol.62, no.6, pp.687-704, June 1974.

[14] Pusone, E.G.; van Genderen, P.; Ligthart, L.P.; van Sinttruijen, J.S, 'A calibration method for polarimetric radar surveillance in a multi-path sea environment.', *2002 32nd European Microwave Conference*, vol., no., pp.1-4, 23-26 Sept. 2002.